Accepted Manuscript

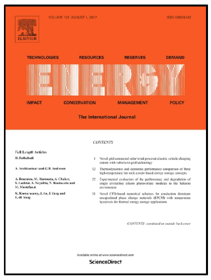

Investigation of the effect of geometric and operating parameters on thermal behavior of vertical shell-and-tube latent heat energy storage systems

Saeid Seddegh, Xiaolin Wang, Mahmood Mastani Joybari, Fariborz Haghighat

PII:	S0360-5442(17)31188-X
DOI:	10.1016/j.energy.2017.07.014
Reference:	EGY 11202
To appear in:	*Energy*
Received Date:	19 January 2017
Revised Date:	29 June 2017
Accepted Date:	04 July 2017

Please cite this article as: Saeid Seddegh, Xiaolin Wang, Mahmood Mastani Joybari, Fariborz Haghighat, Investigation of the effect of geometric and operating parameters on thermal behavior of vertical shell-and-tube latent heat energy storage systems, *Energy* (2017), doi: 10.1016/j.energy.2017.07.014

Investigation of the effect of geometric and operating parameters on thermal behavior of vertical shell-and-tube latent heat energy storage systems

Saeid Seddegh[a], Xiaolin Wang[a*], Mahmood Mastani Joybari[b], Fariborz Haghighat[b]

[a] School of Engineering & ICT, University of Tasmania, Hobart, TAS 7001, Australia.

[b] Department of Building, Civil and Environmental Engineering, Concordia University, Montreal, Quebec H3G 1M8, Canada.

Corresponding author, Email: xiaolin.wang@utas.edu.au; Tel: 61-3-62262133;

Fax: 61-3-62267247

Abstract

In this study, the effect of the geometrical and operational parameters on vertical cylindrical shell-and-tube LHTES systems is investigated. Four different ratios of the shell-to-tube radius are considered with the phase change material (PCM) on the shell side and the heat transfer fluid (HTF) flowing through the tube. The PCM temperature distributions are measured and compared experimentally among the studied storage units. A weighting method is utilized to calculate the average PCM temperature, liquid fraction, and stored energy fraction to evaluate the performance of the storage units. The results show that a shell to tube radius ratio of 5.4 offers better system performance in terms of the charging time and stored energy in the studied LHTES systems. Furthermore, the effects of HTF flow rate and temperature on the storage performance are studied. The HTF flow rate does not show a significant effect on the storage performance; however, the HTF temperature shows large impacts on the charging time. As the HTF temperature increases from 70 to 80 °C, the charging time reduces by up to 68% depending on the radius ratio.

Keywords: latent heat thermal energy storage, phase change material, geometrical parameter, shell-and-tube, heat exchanger

Nomenclature

C_p	Specific heat	$(kJ \cdot kg^{-1} \cdot K^{-1})$
k	Thermal conductivity	$(W \cdot m^{-1} \cdot K^{-1})$
L	Length	(m)
m	PCM mass	(kg)
Q	Stored energy	(kJ)
Q_f	Stored energy fraction	(-)
Q_{max}	Maximum stored energy	(kJ)
R	Pipe radius	(m)
Re	Reynolds number	(-)
t	Time	(s)
T	Temperature	(°C)
V	Volume	(m^3)
Greek letters		
γ	Liquid fraction	(-)
ω	Weight factor	(-)
λ	Latent heat	$(kJ \cdot kg^{-1})$
Subscripts		
i	Inner, node	
l	Liquid, liquidus	
o	Outer	
s	Solid, Solidus	
t	Total	
0	Initial	

1. Introduction

Latent heat thermal energy storage (LHTES) technology has gained extensive attention in many solar energy applications by providing a reservoir of energy to solve the temporal mismatch between solar energy supply and demand [1-8]. Among all different types of LHTES units, the shell-and-tube system is the most intensely researched accounting for more than 70% of the systems studied due to its design simplicity and minimal heat loss from the system [9]. Much research has focused on investigating the effect of geometric and operating parameters on the storage system performance. Cao and Faghri [10] conducted a pioneering numerical investigation on the effect of geometric parameters such as shell radius and tube length. It was found that larger shell radius and longer tube length resulted in higher energy storage; however, this dropped the energy storage density. Lacroix [11] performed a numerical study on a shell-and-tube LHTES system using *n*-octadecane (melting temperature of 26 °C) at the shell side as the PCM and water as the HTF flowing inside the tubes. The results showed that the whole PCM melting time depended not only upon thermal and geometric parameters, but also on the PCM thermophysical properties. The same author evaluated the effect of shell radius, HTF mass flow rate and temperature for tubes with/without fins [12]. Three different shell radii were investigated while the inner tube radius was kept constant. It was observed that for higher shell radii, the PCM was either partially melted or undesirably stored sensible heat only. Bellecci and Conti [13, 14] conducted numerical studies for size optimization of a horizontal solar receiver unit considering different shell radii. It was reported that outer radius (R_o) played a crucial role in the efficient performance of the thermal storage system. There was a certain R_o below which the PCM underwent sensible heat transfer (superheating or sub-cooling) and beyond that part of the PCM did not participate in the phase change process [13]. Furthermore, under the investigated conditions, it was found that a large portion of the PCM could not undergo a phase change at all when the outer to inner tube radius ratio (R_o/R_i) was larger than 4 [14]. Similar results were observed when a eutectic mixture (LiF-MgF_2) was used as the PCM [15]. Esen et al. [16] conducted a series of numerical simulations to investigate the effects of various PCMs, shell and tube radii, PCM volume, HTF mass flow rate and temperature on the charging time. The results indicated that the stored energy raised as the HTF inlet temperature increased. Further, Ismail and his collaborators [17, 18] developed a two-dimensional model to study the effect of the outer shell to inner tube radius ratio (R_o/R_i) on the thermal performance of a PCM in a vertical cylinder. The results indicated that the solidification mass fraction decreased and the time necessary for the complete fusion increased by increasing R_o/R_i. Trp et al. [19, 20] performed a numerical study to evaluate the influence of tube length, shell radius, as well as HTF inlet velocity and temperature on the amount of the stored and recovered energy during the charging and discharging processes. It was concluded that the selection of operating conditions and geometrical parameters depended on the required heat transfer rate and the time by which the energy was to be stored or delivered. Rathod and Banerjee [21, 22] experimentally investigated the effect of HTF mass flow rate and temperature on the thermal performance of a shell-and-tube heat exchanger with PCM at its shell side. The results showed that increasing the HTF mass flow rate and temperature decreased the melting time. Similar results were reported by Gong and Mujumdar [23], and Tao and He [24]. Moreover, considering constant cross-sectional area ($R_o^2 - R_i^2$ = constant), Tao et al. [25, 26] investigated the effect of shell radius variation on melting time. It was found that increasing the shell radius resulted in the longer phase change process, which was attributed to the HTF velocity drop and its consequent heat transfer reduction.

Avci and Yazici [27] experimentally recorded the time histories of paraffin (P56-58) PCM in a horizontal shell-and-tube heat exchanger LHTES. It was reported that increasing (for the charging process) and decreasing (for the discharging process) the HTF inlet temperature enhanced PCM melting and solidification, respectively. Hosseini et al. [28] experimentally and computationally investigated the heat transfer characteristics of a horizontal shell-and-tube heat exchanger LHTES system using RT50 as the PCM. It was revealed that as the inlet HTF temperature increased from 70 to 80 °C, the total melting time decreased by 37%, and the theoretical efficiency in charging and discharging processes raised from 81.1% to 88.4% and from 79.7% to 81.4%, respectively. Seddegh et al. [29] compared heat transfer in horizontal and vertical shell-and-tube LHTES systems, and reported that the hot HTF inlet temperature had a great impact on the heat transfer in both horizontal and vertical systems. However, the HTF flow rate had a negligible effect on charging and discharging processes in the LHTES units.

El-Sawi et al. [30] investigated the effect of HTF temperature, HTF flow rate and storage length on the thermal performance of a centralized LHTES using RT20 as the PCM. It was reported that longer storages could store higher amounts of energy; however, the effect of HTF flow rate was negligible. Furthermore, the highest energy recovery was found to be for cases having an HTF inlet temperature which was 10 °C above the mean PCM phase change temperature [31]. Wang et al. [32] numerically investigated the effects of HTF inlet temperature and mass flow rate on a horizontal shell-and-tube heat exchanger LHTES. The results showed that the HTF inlet temperature greatly affected the time required to complete the charging or discharging process. However, the HTF mass flow rate had little influence on the amount of stored energy, whereas the time needed to complete the charging or discharging process decreased nonlinearly as the HTF mass flow rate increased. They also found that a longer storage had lower energy efficiency ratio, but higher heat storage rate [33]. However, increasing the shell radius decreased both the energy efficiency ratio and the heat storage rate. Thus, further research is needed to investigate the impact of the shell radius on the system performance.

More recently, Tehrani et al. [34] reviewed low to medium temperature shell-and-tube LHTES systems and reported that the majority of the studies were numerical. Table 1 detailed the current research on the shell-and-tube LHTES systems. The only experimental study (highlighted in the table) investigating the geometrical parameters in a vertical cylindrical shell-and-tube storage considered constant tube radius and variable shell radius [16]. In this study, the effect of geometric and operating parameters on a vertical shell-and-tube LHTES system is investigated. An experimental setup is developed for this purpose. Four LHTES units with the same shell radius but variable HTF tube radius are investigated under different HTF temperature and flow rates. Maintaining the shell radius minimizes the effect of the PCM mass change on the storage performance. This has not been investigated in any literature. The temporal variations of experimental temperature in four LHTES units are measured. A new weighting mathematical method is developed to calculate the PCM average temperature, liquid fraction and stored/released energy fraction using the experimental PCM temperatures. These parameters are then used to determine the effect of geometric and operating parameters on the storage performance of the studied LHTES units. The optimal shell to tube radius ratio is investigated. Both the research method and finding have not been reported in other literature. The research provides useful information and guidance to researchers and engineers for design and optimization of vertical shell-and-tube LHTES systems.

Insert Table 1

2. Experimental setup

Fig. 1 shows the experimental setup which was used in this study. It consisted of a hot water tank, a cold water tank, PCM storage unit, hot and cold water pumps, a flow meter, a data acquisition module, thermocouples, valves and extensive piping systems. Water was used as both the hot and cold HTFs.

The PCM storage unit was made of a single pass shell-and-tube heat exchanger. Four cylinders of 0.5 m height and 0.0512 m shell radius (R_o) with different HTF tube radii (R_i) of 0.00635 m, 0.00953 m, 0.01252 m, and 0.01905 m were constructed. The PCM was stored in the annulus, while the HTF passed through the inner tube (see Fig. 1) from top to bottom. All cylinders were made of transparent polypropylene (with thermal conductivity k of 0.1 W/m·K) with a thickness of 0.006 m to allow observation of the melting process. The cylinders were insulated with Armaflex sheets with a thickness of 0.02 m and a thermal conductivity of 0.036 W/m·K. The maximum heat loss of the system at a hot water temperature 80 °C is around 10 W. Table 2 shows the specifications of each studied shell-and-tube unit.

Insert Fig. 1

Insert Table 2

The PCM temperatures inside the four cylinders were measured by Type-T thermocouples with an accuracy of ±0.2 °C. Eight thermocouples were mounted inside each PCM cylinder as shown in Fig. 2 to monitor the temperature during the phase change process. In order to compare the PCM thermal behavior between these vertical cylindrical containers, four thermocouples were located at four levels with the same radial position being 20 mm away from the outer surface of the HTF tube. Another four thermocouples were located at the same four levels in the same radial position but being 5 mm away from the inner surface of the cylinder to study the PCM status.

Insert Fig. 2

During the charging process, the hot HTF was heated up to a pre-set temperature in a hot water tank with a capacity of 108 L using two 2.4 kW thermal electric immersion heaters (model number: TWI50240) with externally adjustable thermostats. The hot water was circulated by a Grundfos vertical, multistage centrifugal pump (model number: CR 1-4 A-A-A-E-HQQE) through the tube in the PCM cylinder where PCM was packed between the tube and cylindrical shell. The hot water flowed from top to the bottom of the tube and was channeled back to the hot water tank from the storage outlet. During the discharging process, the cold water was maintained at the required temperature by a 20 kW chiller (model number: HWP020-3BB) in a 1,575 L capacity cold tank. The cold water was circulated by an Onga horizontal, centrifugal pump (model number: 413) through the tube (from top to bottom) in the PCM cylinder to cool the PCM. A Flomec oval gear positive-displacement flow meter with pulse output was placed in position between the cylinder outlets and hot/cold water tanks to monitor the hot and cold water flow rates. Moreover, temperatures and water flow rates were recorded by a data acquisition system at 2.5 second time intervals (National Instruments NI9411). The PCM used in the study was RT60 paraffin wax from Rubitherm GmbH. The PCM thermophysical properties and testing conditions are listed in Table 3.

Insert Table 3

3. Experimental data reduction

In order to compare the performance of the different storage units, three parameters (i.e. average PCM temperature, liquid fraction, and stored energy fraction) were introduced and utilized in the study. These three parameters were calculated using a newly developed weighting method which is similar to that reported in our recent publication [36]. The similar weighting method was also used by Caron-Soupart et al. [37]. They used an interpolation and extrapolation to obtain temperature values for some cells in the performance analysis of thermal energy storage using phase change material. In our study, the direct experimental data was used to determine the cells' temperature. The method was detailed below.

Insert Fig. 3

As presented earlier, the positions of the thermocouples were distributed at different locations which were altered based on the tube radius in each experimental setup. Therefore, the control volume around each node (see Fig. 3) had a different area (volume) due to the thermocouple location in each test. A weight factor (ω) is then defined to take into account the volume of the PCM, which is approximated by the corresponding node (thermocouple). Thus, for node *i*:

$$\omega_i = \frac{V_i}{V_t} \tag{1}$$

where V_i is the volume of the control volume surrounding node *i* as depicted in Fig. 3 and V_t are the total PCM storage volume. Thus, having the locally measured temperature values (T_i), the average temperature of the storage is calculated by:

$$T = \sum_i \omega_i T_i \tag{2}$$

The liquid fraction at each thermocouple location is calculated where each location is accounted as a separate node with its actual available temperature value. Therefore, according to the measured temperature (T_i) at each node, three different options are possible based on which the liquid fraction at each node is calculated:

$$\gamma_i = \begin{cases} 0 & T_i < T_s \\ \dfrac{T_i - T_s}{T_l - T_s} & T_s < T_i < T_l \\ 1 & T_i > T_l \end{cases} \tag{3}$$

where T_s and T_l are the solidus and liquidus temperatures, respectively. Once the nodal liquid fraction values are calculated, the average liquid fraction would be:

$$\gamma = \sum_i \omega_i \gamma_i \tag{4}$$

To calculate the stored energy of the PCM, the same weighting approach was applied to the nodal temperatures. The stored energy by each node was calculated by:

$$Q_i = \begin{cases} mC_{p,s}\left(T_i - T_0\right) & T_i < T_s \\ mC_{p,s}\left(T_s - T_0\right) + m\gamma_i\lambda & T_s < T_i < T_l \\ mC_{p,s}\left(T_s - T_0\right) + m\lambda + mC_{p,l}\left(T_i - T_l\right) & T_i > T_l \end{cases} \quad (5)$$

where T_0 is the initial temperature of the PCM storage (15 °C), which is used for both charging and discharging processes. According to Table 3, two different HTF temperatures of 70 and 80 °C are used in this study. Consequently, the final PCM temperature after the charging process would be different not only among the cylinders, but also according to the corresponding HTF temperature. In order to prevent ambiguity and enable solid comparison of the results, the initial PCM temperature (15 °C) is considered constant in Equation (5). In this way, under charging condition, the stored energy of the cylinders initiates from zero and reaches a maximum value (Q_{max}), while under discharging process, the stored energy declines from the maximum value back to zero. Then, the total stored energy of the PCM is calculated using the weight factor:

$$Q = \sum_i \omega_i Q_i \quad (6)$$

Finally, the stored energy fraction would be:

$$Q_f = \frac{Q}{Q_{max}} \quad (7)$$

In order to have a smooth transition of the average temperature, liquid fraction and stored energy fraction values, curve fitting has been applied to the experimental data. As an example, Fig. 4 shows the fitted curve along with the experimental data for the liquid fraction values of Cylinder D. Furthermore, according to the error propagation [38], the uncertainty level of the stored energy can be calculated based on the measurement uncertainty of temperatures. The maximum uncertainty is ±3.6%.

Insert Fig. 4

4. Results and discussion

The thermal behavior of the four different LHTES systems is investigated and compared under different operating conditions in the following sections.

4.1. Charging process

4.1.1. Charging process – 5 mm thermocouples

Fig. 5 (a-d) shows temperature variations in thermocouple probes located 5 mm away from the inner surface of the acrylic cylinder within each container under the charging HTF temperature of 80 °C and the flow rate of 10 L/min. It is seen that PCM temperatures at different levels reach the melting temperature at different times. The time needed for the PCM to melt for higher levels is shorter than that of the lower ones. This is due to the natural convection as reported in the literature [29]. It should be noted that the entire mass of PCM in each cylinder was completely melted once the thermocouple located 5 mm away from the inner surface of the acrylic cylinder at level 1 reached a stable temperature above the PCM melting temperature. The total charging time is defined as all thermocouple temperatures reach a stable temperature during a charging process. Comparing the total charging time for different cylinders shows that increasing the HTF tube radius reduces the required charging time. The charging time reduced by up to 38% as the shell to tube radius ratio decreased from 8.1 to 2.7 in Cylinders A to D. This decrease in total charging time is due to a few reasons: The first reason is because of the fact that the larger HTF tube radius provides larger heat transfer surface area; hence, larger heat transfer rate which reduces charging time. The second reason is due to a reduction in the total mass of the PCM. As the HTF tube radius increases from Cylinders A to D, the total mass of the PCM in the cylinder decreases by 12.5% which reduces the total charging temperature as well. The third reason is heat transfer distance from the HTF tube surface to the inner surface of the shell. This effect is very small in comparison to the first two reasons. Due to the natural convection, the liquid PCM moves up to the upper part of the system and natural convection enhances the heat transfer in the liquid PCM along with the radial direction.

Insert Fig. 5

4.1.2. Charging process – 20 mm thermocouples

Fig. 6 (a-d) compares temperature variations of thermocouple probes located 20 mm away from the HTF tube at each level for the HTF charging temperature of 80 °C and flow rate of 10 L/min. As the tube radius increases from Cylinder A to D, the melting time decreases. This demonstrates the significant effect of the HTF tube surface area on the heat transfer in the PCM. It also shows that the time difference to reach the melting point decreased from 7 hours at level 1 to 2.5 hours at level 4 as the radius increases from Cylinder A to D. This reveals that at higher levels, the influence of the radius ratio decreases as the time delay reduces, which is due to two reasons. First, natural convection enhances the heat transfer at the higher PCM levels. Second, the PCM mass in a cylinder with smaller HTF tube radius is more than that of a cylinder with larger HTF tube radius. This excess PCM in the cylinders with smaller HTF tube radius requires more energy and consequently longer time to melt. As the level moves from the top to the bottom, the difference of PCM mass increases among the cylinders and hence the difference of the total melting time accumulates. Thus, the time difference at the lower levels is longer.

Furthermore, in both Figs. 5 and 6, the remarkable change in the slope of temperature variation with time is at a temperature much lower than the melting temperature point (55 - 61 °C). This is mainly due to natural convection which substantially enhanced the heat transfer rate and affected the increasing rate of the PCM temperature with time. The similar finding was reported in an experimental investigation on latent heat storage using paraffin wax as phase change material by Rathod and Banerjee [39, 40]. In our recent publication [1], the temperature variation of the PCM was theoretically investigated in a shell-and-tube thermal energy storage system using conduction only heat transfer model and combined conduction & convection heat transfer model. In the combined heat transfer model, the slope of the temperature variation with time is similar to the experimental data presented in this study. This result further approved that the remarkable change in the slope of temperature variation with time at a lower temperature is due to natural convection.

Insert Fig. 6

4.1.3. Charging process – Comparison

Fig. 7 (a-c) compares the average PCM temperature, liquid fraction, and stored energy fraction of the LHTES systems during the charging process with the HTF temperature of 80 °C and the flow rate of 10 L/min. The results show that the trends in all cylinders are similar. However, among the cylinders, Cylinder A with the largest shell to tube radius ratio, has the slowest energy storage process and its average PCM temperature rise, liquid fraction rise and energy storage rate are much slower than others. On the other hand, Fig. 7c shows that the increasing rate in energy storage decreases as the shell to tube radius ratio decreases from 8.1 to 2.7. For example, during the first 5 hrs, as the radius ratio decreased from Cylinder A (8.1) to B (5.4), the stored energy fraction increased from 0.375 to 0.64 while it only increased from 0.75 to 0.85 as the radius ratio decreased from Cylinder C (4.0) to Cylinder D (2.7). It is clear that the increasing rate in energy storage from Cylinder C to D is much lower than that from Cylinder A to B. These results indicate that an optimal shell to tube radius ratio exists. If the shell to tube radius ratio is too small, the energy storage rate is very low. On the other hand, if the ratio is too large, it wastes the initial cost and lowers the total stored energy since larger HTF tube reduces the amount of PCM in the system. The detailed discussion on the optimal ratio is presented in Section 5.

Insert Fig. 7

4.2. Discharging process

Upon completion of the charging process, the cylinders were immediately discharged by passing the cold HTF at a temperature of 10 °C and flow rate of 10 L/min.

4.2.1. Discharging process – 5 mm thermocouples

Fig. 8 (a-d) shows the temperature variation in thermocouple probes located 5 mm away from the inner surface of the acrylic cylinder within each cylinder during the discharging process. The discharging process finishes when the temperatures at all four levels reach a stable temperature. This time is considered as the whole discharging time. The results show that the required discharging time is reduced by up to 44% as the shell to tube radius ratio decreases from 8.1 to 2.7. This reduction is mainly due to the following reasons: (i) the heat transfer area increases as the shell to tube radius ratio decreases. The increase in heat transfer area enhances the heat transfer rate and hence reduces the discharging time. (ii) The mass of PCM decreases with decreasing shell to tube radius ratio. The largest variation of the PCM mass between the cylinders with the largest and smallest HTF tubes is about 12.5%. This mass difference also contributes to the different solidification time. (iii) The distance between the HTF outer surface to the inner surface of the shell also contributes to the difference in the discharging time. Since the change of distance is very small, this effect is relatively small in comparison to the other two. Furthermore, Fig. 8 also shows that the PCM at different thermocouple locations solidifies almost at the same time. According to the literature [1], this indicates that thermal conduction dominates the heat transfer in the discharging process.

Insert Fig. 8

4.2.2. Discharging process – 20 mm thermocouples

Fig. 9 (a-d) compares the temperature variation at each level for the thermocouple probes located 20 mm away from the HTF tube. It is obvious that the PCM temperature decreases much faster in a cylinder with larger tube radius. This is due to the larger heat transfer area, which increases the heat transfer rate despite increase in the PCM mass due to increase in the HTF tube radius. During discharging process, the solidified PCM surrounds the HTF tube; thus, the thermal energy exchange from the high-temperature PCM to the cold HTF could only be transferred via thermal conduction. Therefore, the heat transfer surface area plays a very important role in the discharging process. As the heat transfer area increases from Cylinder A to D, the heat transfer rate increases inside the Cylinder A to D. Therefore, the shapes and lengths of solidification plateau are different among the Cylinders A to D. It is also noted that shape and lengths of the solidification plateau are different at different levels in the same cylinder. This is mainly due to the natural convection which moves the liquid PCM up and solidifies the PCM from bottom to the top.

Insert Fig. 9

4.2.3. Discharging process – Comparison

Fig. 10 (a-c) compares the average PCM temperature, liquid fraction, and stored energy fraction of the LHTES systems during the discharging process. As the shell to tube radius ratio decreases from 8.1 (Cylinder A) to 2.7 (Cylinder D), the rate of the average PCM temperature drop increases. This is mainly due to the large heat transfer rate caused by the large heat transfer area in the cylinder with the large tube radius. Fig. 10b shows that the solidification processes in all cylinders are much faster than the melting processes as shown in Fig. 7b. This is mainly due to the temperature difference between the HTF and PCM phase change temperatures which was much higher for the discharging process as compared to the charging one. This also explains why the energy release in the discharging process is faster than the energy storage in the charging process as shown in Fig. 10c.

Insert Fig. 10

4.3. Effect of operating parameters

4.3.1. HTF temperature

Fig. 11 (a-d) shows the variation of PCM temperature in a complete charging and discharging cycle for thermocouple probes located 5 mm from the inner surface of the acrylic shell for each cylinder. The charging or discharging process was continued until the PCM temperature in all thermocouples did not change significantly. Two different HTF charging temperatures of 70 °C and 80 °C were considered with the same discharging temperature of 10 °C while the HTF flow rate was kept at 10 L/min. It is observed that the overall charging-discharging time is highly dependent on the charging time, which is influenced by the HTF temperature. During the charging process, as the HTF temperature increased from 70 to 80 °C, the total charging time reduced by 68%, 63%, 60%, and 54% in Cylinders A, B, C, and D, respectively. However, during the discharging process with the HTF temperature of 10 °C after being charged with HTF at 70 °C and 80 °C, the PCM temperature drops rapidly and the HTF changing temperature has no significant effect on the discharging process. As the shell to tube radius ratio reduced from 8.1 to 2.7 between Cylinders A and D, the overall cycle time decreased by 34% and 40% for the HTF temperature of 70 to 80 °C, respectively. Furthermore, it is also found that the stable PCM temperature is lower than the HTF inlet temperature during the charging process. This is mainly due to the two reasons. First, when all PCM was melted, the effect of natural convection reduces and hence the heat transfer between the HTF fluid and liquid PCM reduces. This lowers the energy transfer into the PCM. Second, the inevitable heat loss from the system to the environment, which prevents the PCM temperature from increasing.

Insert Fig. 11

Fig. 12 (a-c) compares the average PCM temperature, liquid fraction, and stored energy fraction of the LHTES systems during the complete charging-discharging process with the

HTF charging temperature of 70 and 80 °C. The results showed that the charging HTF temperature largely affected the charging time and total amount of energy storage. As the charging HTF temperature increased from 70 to 80 °C, the charging time reduced by more than 50% and the total stored energy increased by up to 20%. Furthermore, the results revealed that the effect on charging time in the system with the large shell to tube radius ratio was much larger than that in the system with the small radius ratio.

Insert Fig. 12

4.3.2. HTF flow rate

All previous presented experimental data were performed at the HTF flow rate of 10 L/min. This flow rate ensures turbulent flow with the Reynolds number of 47225, 31400, 23612, and 15741 in Cylinders A, B, C, and D, respectively. In order to investigate the effect of HTF flow rate on the system energy storage performance, the experiments were also performed under different HTF mass flow rates with a constant HTF Reynolds number (23612, turbulent flow regime) among cylinders. Table 4 compares the charging and discharging times in different cylinders at the charging HTF temperature of 70 °C, and discharging HTF temperature of 10 °C under two scenarios: constant HTF Reynolds number with variable flow rates, and constant flow rate of 10 L/min with different Reynolds numbers. At the constant Reynolds number of 23612, the corresponding flow rates were 5, 7.5, 10, and 15 L/min in Cylinders A, B, C, and D, respectively. This approach produces the same Nusselt number in all tubes in the storage system. As the shell to tube radius ratio decreased from 8.1 to 2.7 between the Cylinder A and D, the charging, discharging and complete cycle times decreased by 28%, 44% and 34%, respectively at both scenarios. Furthermore, the charging and discharge times were almost the same in the same cylinder under different flow rates. These comparison results indicated that the HTF flow rate has no significant effect on the charging and discharging processes. This can be explained by the heat transfer coefficient. In the storage systems, the heat transfer coefficient between the HTF and tube surface was much larger than that between the tube surface and PCM. The heat transfer rate was dominated by the heat transfer coefficient between the tube surface and PCM. Therefore, increasing heat transfer rate by varying the HTF flow rate did not change the overall heat transfer from the HTF flow to the PCM in the storage systems.

Insert Table 4

5. Optimal shell to tube radius ratio

Fig. 13 shows the variation of the charging and discharging times, stored energy and average energy storage rate under different HTF temperatures and shell to tube radius ratios at the HTF flow rate of 10 L/min. The stored energy at both temperatures is different at all cylinders. This is due to (i) the higher temperature of the PCM leading to higher sensible heat at the same cylinder (Accounting for 60 to 65% of the difference of the stored energy at two temperatures depending on the cylinders) and (ii) the melting that is not complete when the hot HTF temperature is 70 °C (Accounting for about 35 to 40 % of the difference). However, the effect of the geometric parameter on the stored energy is the same at the both temperatures. As the radius ratio increases, the charging as well as discharging time increases. As shown in Fig. 13a, the charging time increases drastically under both HTF temperatures when the radius ratio is larger than 5.4. This result indicated that the optimal shell to tube radius ratio should be less than 5.4 in the studied LHTES systems. Furthermore, as shown in Fig. 13b, as the radius ratio increased beyond 5.4, the increase in stored energy is insignificant. On the other hand, for the radius ratios below 5.4, the stored energy decreased sharply. Fig. 13b also shows that the average energy storage rate dropped from 84 to 40 kJ/hr at 80 °C and from 36 to 16 kJ/hr at 70 °C, respectively as the shell to tube radius ratio increased from 2.7 to 8.1. But the change of the average energy storage rate was more than

40% as the shell to tube radius ratio increased from 5.4 to 8.1 while it was less than 20% as the shell to tube radius ratio increased from 2.7 to 4 and from 4 to 5.4 at both HTF temperatures. By balancing the charging time, stored energy and average energy storage rate in Fig. 13, the optimal shell to tube radius ratio is around 5.4 in the studied configurations.

Insert Fig. 13

6. Conclusion

In this paper, the effects of geometrical and operating parameters on the phase change performance of vertical cylindrical LHTES units were investigated. For this purpose, four different shell to tube radius ratios were considered with the PCM at the shell side and the HTF passing through the tube side. The storages had identical shell radii but different HTF tube radii to investigate the effect of heat transfer surface area on the system storage performance. The PCM temperature distributions were measured and compared experimentally among the considered cylinders. The experimental results and calculated PCM average temperature, liquid fraction, and stored energy fraction showed that complete charging and discharging is highly dependent on the shell to tube radius ratio as well as the HTF temperature while almost independent of the HTF flow rate. By balancing the discharging time and stored energy capacity, the best shell to tube radius ratio was found to be around 5.4 in the studied storage systems. This study provides engineers useful information for the design and optimization of vertical shell-and-tube LHTES systems.

References

[1] S. Seddegh, X. Wang, A.D. Henderson, Numerical investigation of heat transfer mechanism in a vertical shell and tube latent heat energy storage system, Applied Thermal Engineering, 87 (2015) 698-706.

[2] M.M. Joybari, F. Haghighat, J. Moffat, P. Sra, Heat and cold storage using phase change materials in domestic refrigeration systems: The state-of-the-art review, Energy and Buildings, 106 (2015) 111-124.

[3] J. P. da Cunha, P. Eames, Thermal energy storage for low and medium temperature applications using phase change materials – A review, Applied Energy, 177 (2016) 227 - 238.

[4] F. Fornarelli, S.M. Camporeale, B. Fortunato, P. Oresta, L. Magliocchetti, A. Miliozzi, G. Santo, CFD analysis of melting process in a shell-and-tube latent heat storage for concentrated solar power plants, Applied Energy, 164 (2016) 711-722.

[5] Y.B. Tao, V.P. Carey, Effect of PCM thermophysical properties on thermal storage performance of a shell-and-tube latent heat storage unit, Applied Energy, 179 (2016), 203-210.

[6] R. Jacob, M. Belusko, A. Inés Fernández, L. F. Cabeza, W. Saman, F. Bruno, Embodied energy and cost of high temperature thermal energy storage systems for use with concentrated solar power plants, Applied Energy 180 (2016) 586-597.

[7] D. Zhao, G. Tan, Numerical analysis of a shell-and-tube latent heat storage unit with fins for air-conditioning application, Applied Energy, 138 (2015) 381-392.

[8] S. Seddegh, X. Wang, A.D. Henderson, Z. Xing, Solar domestic hot water systems using latent heat energy storage medium: A review, Renewable and Sustainable Energy Reviews, 49 (2015) 517-533.

[9] F. Agyenim, N. Hewitt, P. Eames, M. Smyth, A review of materials, heat transfer and phase change problem formulation for latent heat thermal energy storage systems (LHTESS), Renewable and Sustainable Energy Reviews, 14 (2) (2010) 615-628.

[10] Y. Cao, A. Faghri, Performance characteristics of a thermal energy storage module: a transient PCM/forced convection conjugate analysis, International Journal of Heat and Mass Transfer, 34 (1) (1991) 93-101.

[11] M. Lacroix, Numerical simulation of a shell-and-tube latent heat thermal energy storage unit, Solar Energy, 50 (4) (1993) 357-367.

[12] M. Lacroix, Study of the heat transfer behavior of a latent heat thermal energy storage unit with a finned tube, International Journal of Heat and Mass Transfer, 36 (8) (1993) 2083-2092.

[13] C. Bellecci, M. Conti, Latent heat thermal storage for solar dynamic power generation, Solar Energy, 51 (3) (1993) 169-173.

[14] C. Bellecci, M. Conti, Phase change thermal storage: transient behaviour analysis of a solar receiver/storage module using the enthalpy method, International Journal of Heat and Mass Transfer, 36 (8) (1993) 2157-2163.

[15] C. Bellecci, M. Conti, Transient behaviour analysis of a latent heat thermal storage module, International Journal of Heat and Mass Transfer, 36 (15) (1993) 3851-3857.

[16] M. Esen, A. Durmuş, A. Durmuş, Geometric design of solar-aided latent heat store depending on various parameters and phase change materials, Solar Energy, 62 (1) (1998) 19-28.

[17] K. Ismail, C. Melo, Convection-based model for a PCM vertical storage unit, International Journal of Energy Research, 22 (14) (1998) 1249-1265.

[18] K. Ismail, M. Goncalves, Thermal performance of a PCM storage unit, Energy Conversion and Management, 40 (2) (1999) 115-138.

[19] A. Trp, K. Lenic, B. Frankovic, Analysis of the influence of operating conditions and geometric parameters on heat transfer in water-paraffin shell-and-tube latent thermal energy storage unit, Applied Thermal Engineering, 26 (16) (2006) 1830-1839.

[20] A. Trp, An experimental and numerical investigation of heat transfer during technical grade paraffin melting and solidification in a shell-and-tube latent thermal energy storage unit, Solar Energy, 79 (6) (2005) 648-660.

[21] M. Rathod, J. Banerjee, Experimental investigations on latent heat storage unit using paraffin wax as phase change material, Experimental Heat Transfer, 27 (1) (2014) 40-55.

[22] M.K. Rathod, J. Banerjee, Thermal performance enhancement of shell and tube Latent Heat Storage Unit using longitudinal fins, Applied Thermal Engineering, 75 (2015) 1084-1092.

[23] Z.-X. Gong, A.S. Mujumdar, Finite-element analysis of cyclic heat transfer in a shell-and-tube latent heat energy storage exchanger, Applied Thermal Engineering, 17 (6) (1997) 583-591.

[24] Y. Tao, Y. He, Numerical study on thermal energy storage performance of phase change material under non-steady-state inlet boundary, Applied Energy, 88 (11) (2011) 4172-4179.

[25] Y.-B. Tao, M.-J. Li, Y.-L. He, W.-Q. Tao, Effects of parameters on performance of high temperature molten salt latent heat storage unit, Applied Thermal Engineering, 72 (1) (2014) 48-55.

[26] Y. Tao, Y. He, Z. Qu, Numerical study on performance of molten salt phase change thermal energy storage system with enhanced tubes, Solar Energy, 86 (5) (2012) 1155-1163.

[27] M. Avci, M.Y. Yazici, Experimental study of thermal energy storage characteristics of a paraffin in a horizontal tube-in-shell storage unit, Energy Conversion and Management, 73 (2013) 271-277.

[28] M. Hosseini, M. Rahimi, R. Bahrampoury, Experimental and computational evolution of a shell and tube heat exchanger as a PCM thermal storage system, International Communications in Heat and Mass Transfer, 50 (2014) 128-136.

[29] S. Seddegh, X. Wang, A.D. Henderson, A comparative study of thermal behaviour of a horizontal and vertical shell-and-tube energy storage using phase change materials, Applied Thermal Engineering, 93 (2016) 348-358.

[30] A. El-Sawi, F. Haghighat, H. Akbari, Assessing long-term performance of centralized thermal energy storage system, Applied Thermal Engineering, 62 (2) (2014) 313-321.

[31] A. El-Sawi, F. Haghighat, H. Akbari, Centralized latent heat thermal energy storage system: model development and validation, Energy and Buildings, 65 (2013) 260-271.

[32] W.-W. Wang, K. Zhang, L.-B. Wang, Y.-L. He, Numerical study of the heat charging and discharging characteristics of a shell-and-tube phase change heat storage unit, Applied Thermal Engineering, 58 (1) (2013) 542-553.

[33] W.-W. Wang, L.-B. Wang, Y.-L. He, The energy efficiency ratio of heat storage in one shell-and-one tube phase change thermal energy storage unit, Applied Energy, 138 (2015) 169-182.

[34] S.S.M. Tehrani, R.A. Taylor, P. Saberi, G. Diarce, Design and feasibility of high temperature shell and tube latent heat thermal energy storage system for solar thermal power plants, Renewable Energy, 96 (2016) 120-136.

[35] RT60 Data Sheet. Rubitherm Technologies GmbH, 2017.

[36] M.M. Joybari, F. Haghighat, S. Seddegh, Numerical simulation of a triplex tube heat exchanger with phase change material: Simultaneous charging and discharging, Energy and Buildings, 139 (2017) 426-438.

[37]A. Caron-Soupart, J. Fourmigué, P. Marty, R. Couturier, Performance analysis of thermal energy storage systems using phase change material, 98 (2016) 1286-1296.

[38] P.R. Bevington, D.K. Robinson, 2002, Data Reduction and Error Analysis for the Physical Sciences (3rd ed.), McGraw-Hill, ISBN0-07-119926-8.

[39]M.K. Rathod, J. Banerjee, Experimental investigations on latent heat storage using paraffin wax as phase change material, Exp. Heat Transf. J. Therm. Energy Generation, Transp. Storage, Convers. 27 (2014) 40 – 55.

[40] M. K. Rathod, J. Banerjee, Thermal performance enhancement of shell and tube latent heat storage unit using longitudinal fins, Applied Thermal Engineering, 2015, 75, 1084-1092.

Figure captions

Fig. 1 Pictorial views of (a) the whole experimental rig (b) the four PCM storage cylinders

Fig. 2 Locations of thermocouples (bold points)

Fig. 3 Schematic representation of the experimental setup showing the location of thermocouples and the considered control volume.

Fig. 4 Variation of the liquid fraction for Cylinder D under charging showing the fitted curve against the experimental data.

Fig. 5 Comparison of temperatures recorded by thermocouple probes located 5 mm away from the shells during the charging process.

Fig. 6 Comparison of temperatures of thermocouples located 20 mm away from the HTF tubes during the charging process.

Fig. 7 Comparison of the PCM average temperature, liquid fraction, and stored energy fraction during the charging process.

Fig. 8 Comparison of temperatures recorded by thermocouples located 5 mm away from the shells during the discharging process.

Fig. 9 Comparison of temperatures recorded by thermocouples located 20 mm away from the HTF tubes during the discharging process.

Fig. 10 Comparison of the PCM average temperature, liquid fraction, and stored energy fraction during the discharging process.

Fig. 11 Complete charging and discharging cycles for thermocouples located 5 mm away from the shells under different HTF temperatures.

Fig. 12 Comparison of the PCM average temperature, liquid fraction, and stored energy fraction during the complete charging/discharging cycle.

Fig. 13 The effect of the shell to tube radius ratio on the storage system performance under different HTF temperatures.

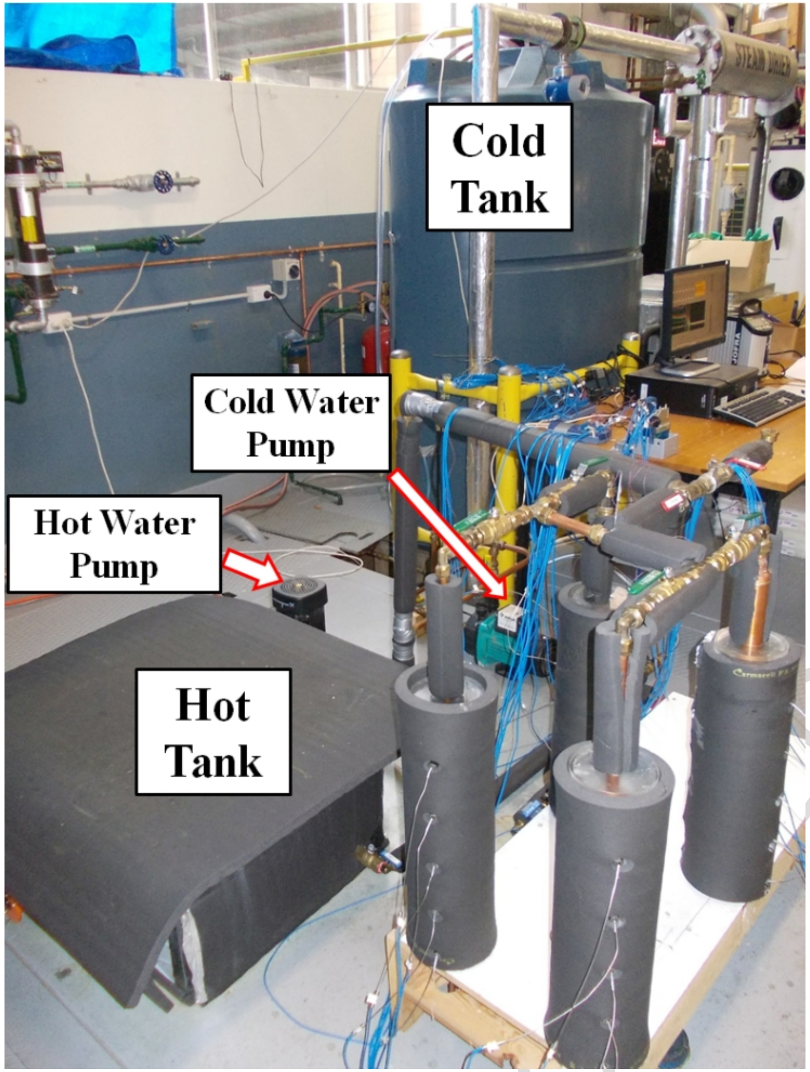

(a)

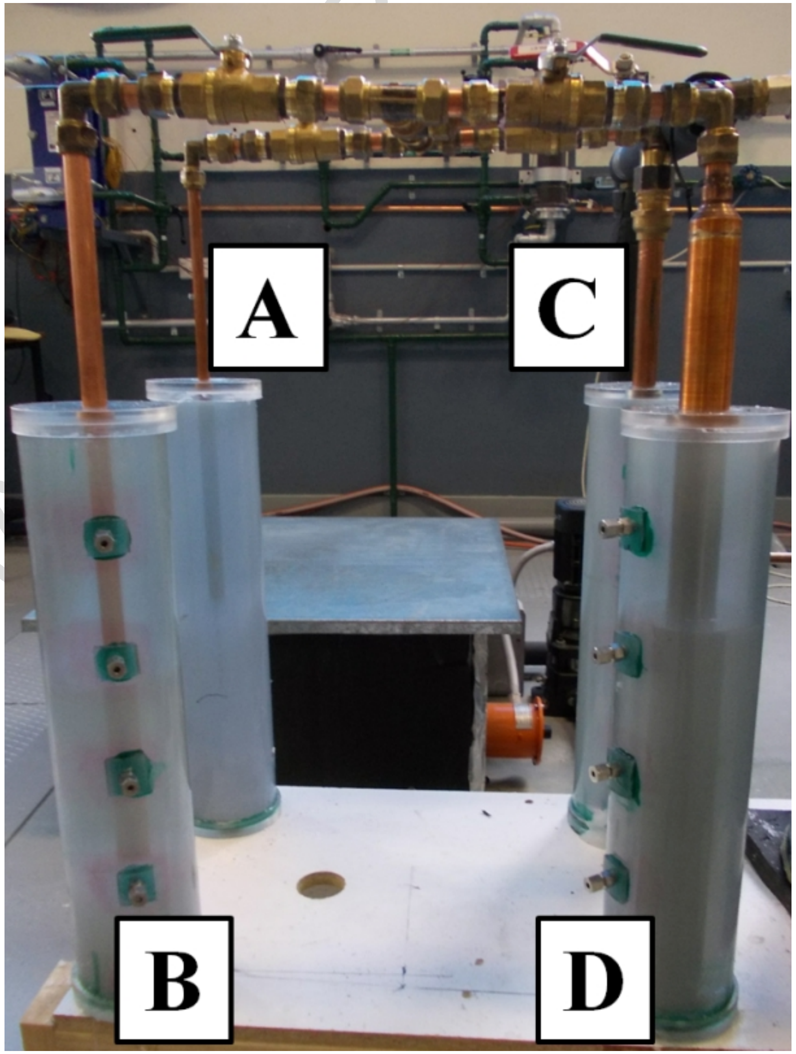

(b)

Fig. 1 Pictorial views of (a) the whole experimental rig (b) the four PCM storage cylinders

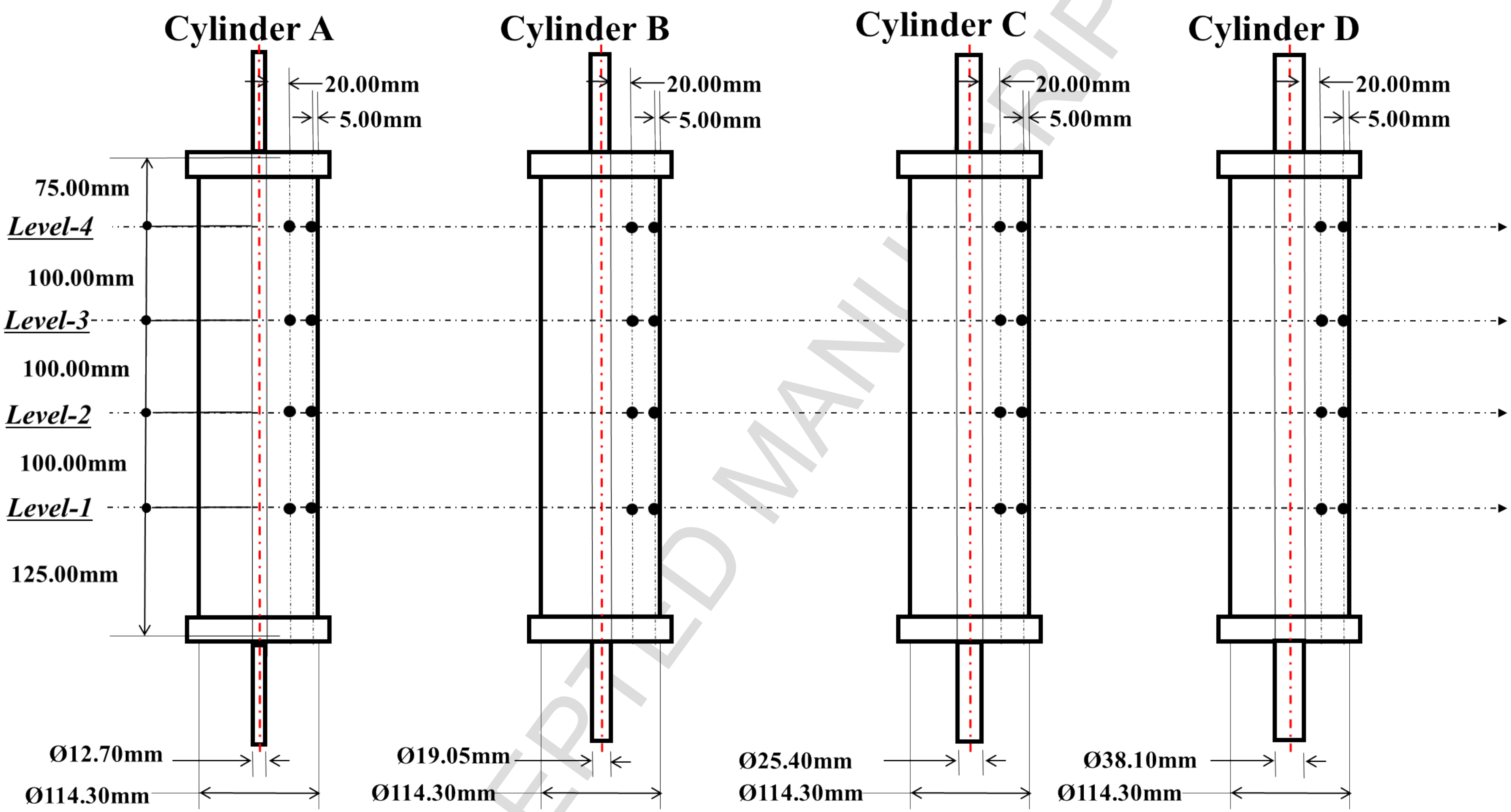

Fig. 2 Locations of thermocouples (bold points)

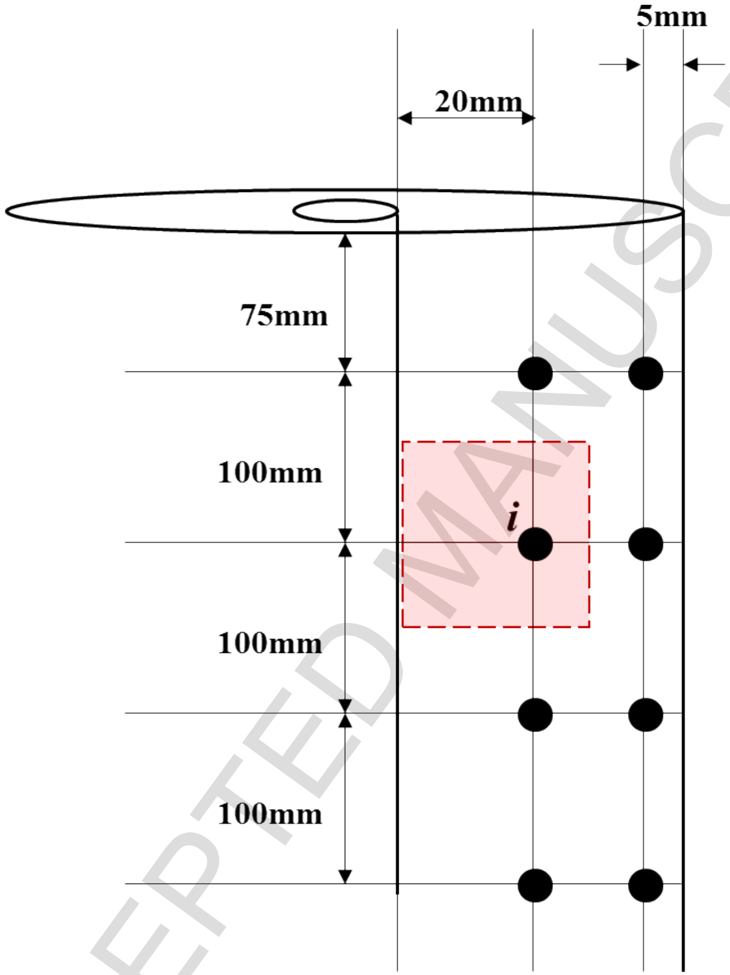

Fig. 3 Schematic representation of the experimental setup showing the location of thermocouples and the considered control volume

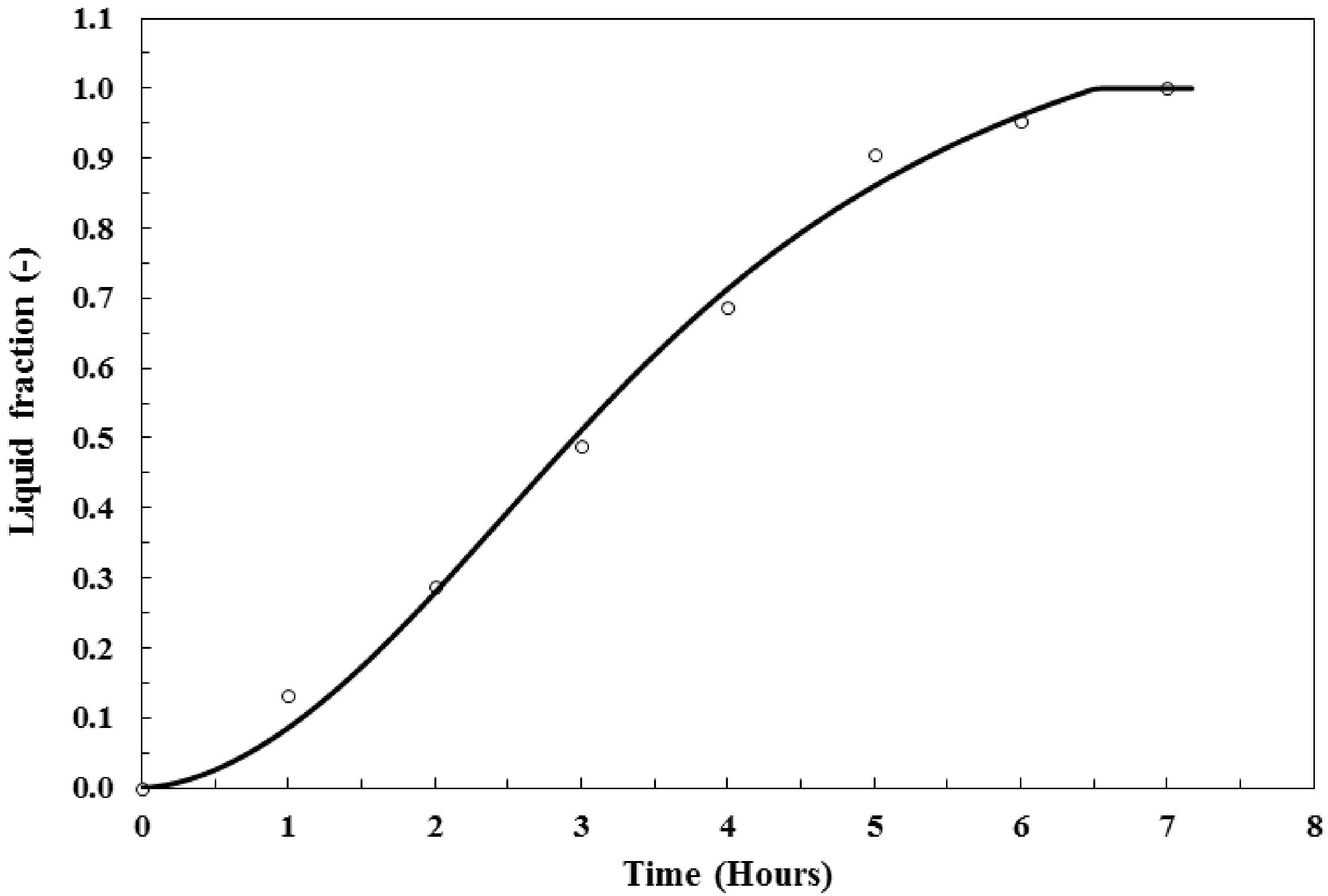

Fig. 4 Variation of the liquid fraction for Cylinder D under charging showing the fitted curve against the experimental data

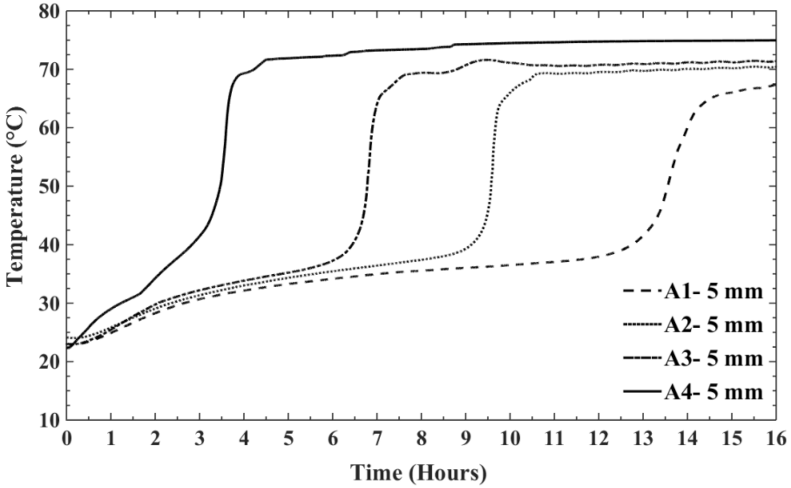

(a) Cylinder A

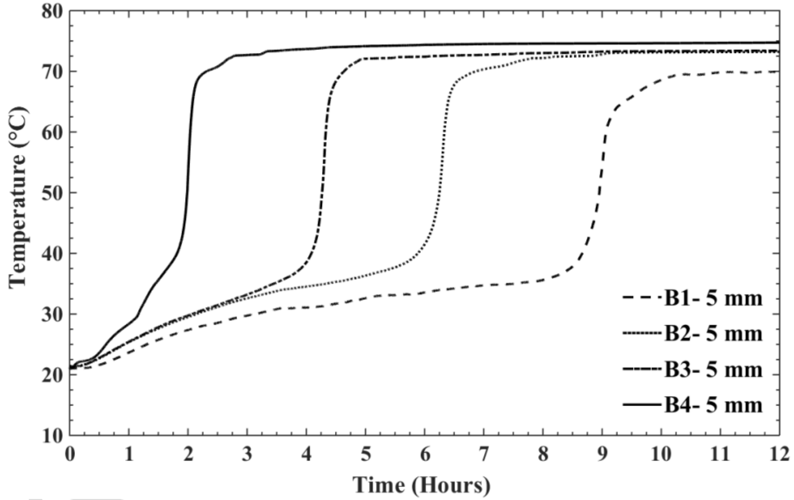

(b) Cylinder B

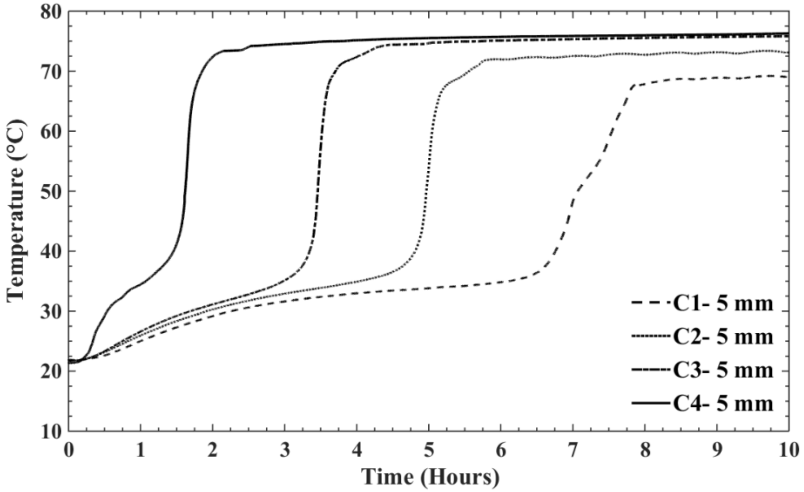

(c) Cylinder C

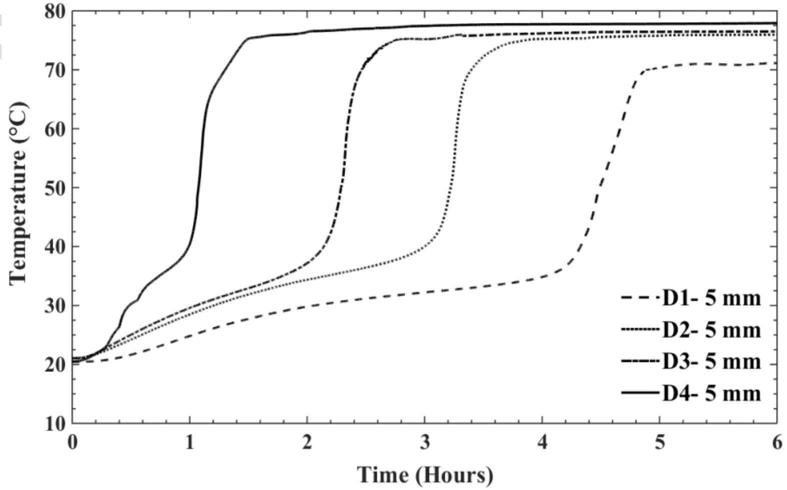

(d) Cylinder D

Fig. 5 Comparison of temperatures recorded by thermocouple probes located 5 mm away from the shells during the charging process

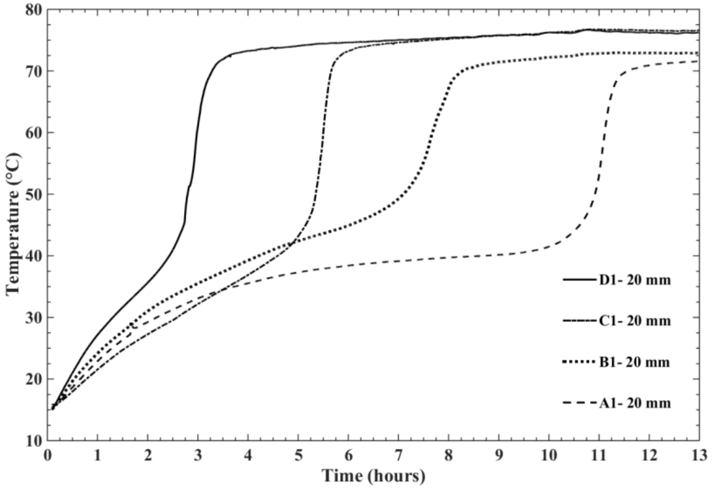

(a) Level 1

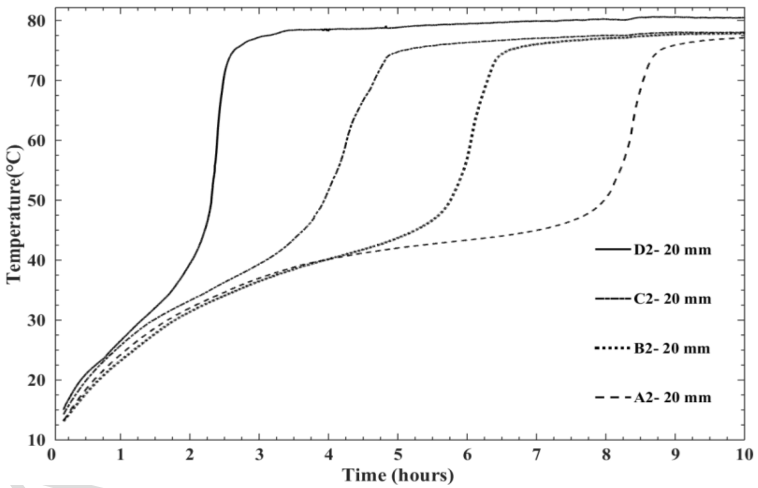

(b) Level 2

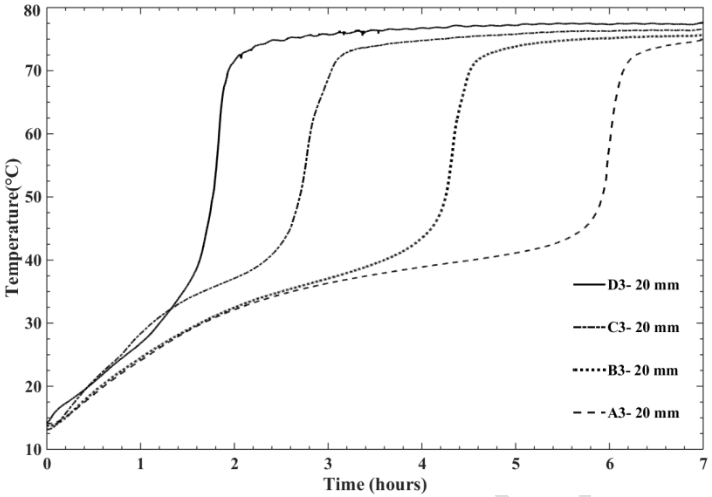

(c) Level 3

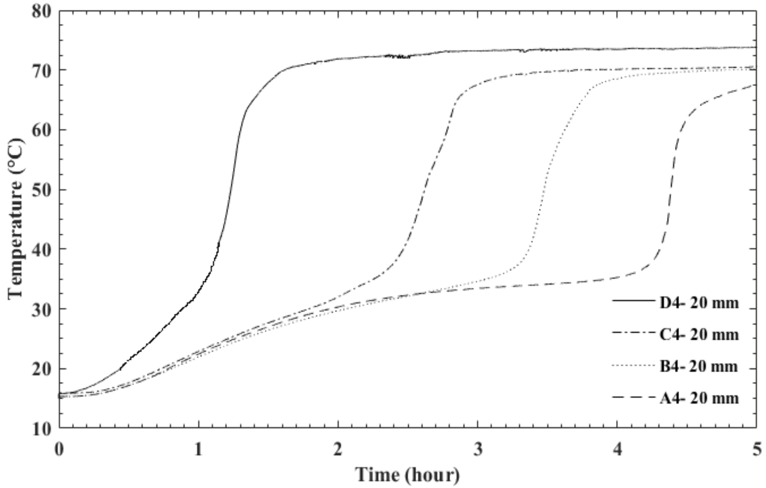

(d) Level 4

Fig. 6 Comparison of temperatures of thermocouples located 20 mm away from the HTF tubes during the charging process

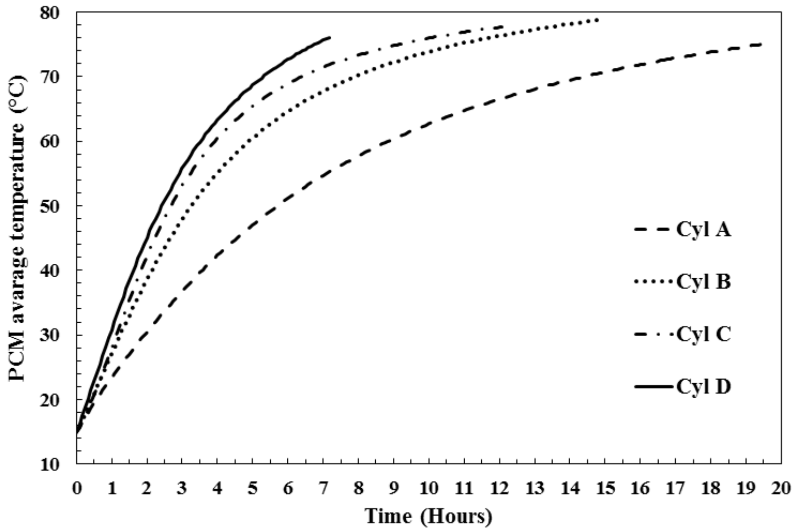

(a) Comparison of average PCM temperature

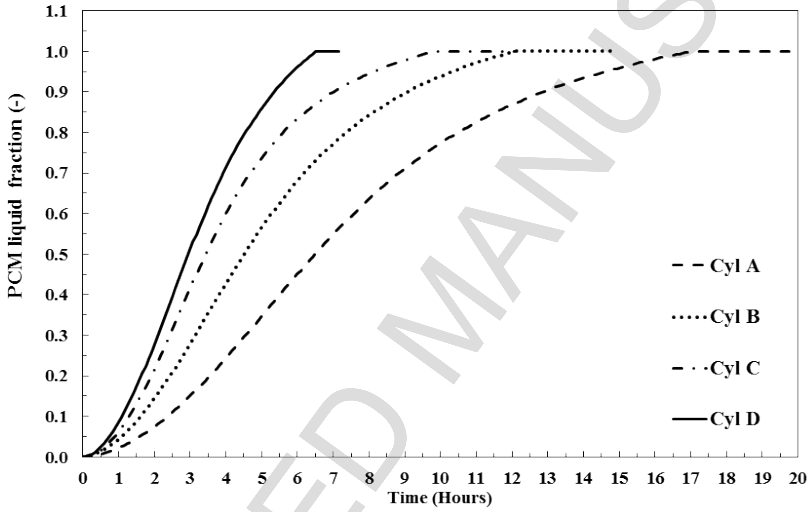

(b) Comparison of PCM liquid fraction

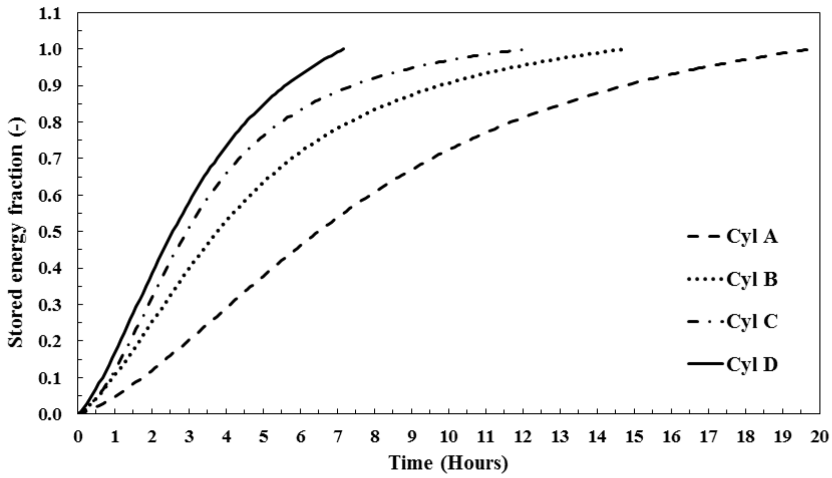

(c) Comparison of stored energy fraction

Fig. 7 Comparison of the PCM average temperature, liquid fraction, and stored energy fraction during the charging process

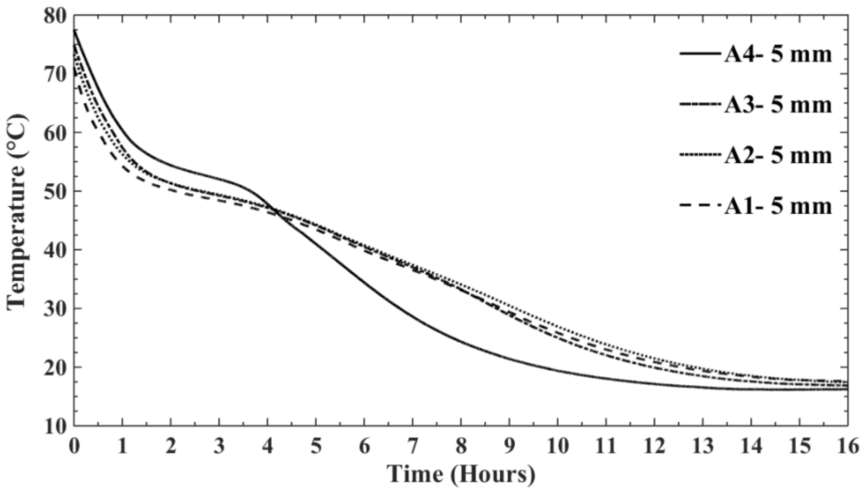

(a) Cylinder A

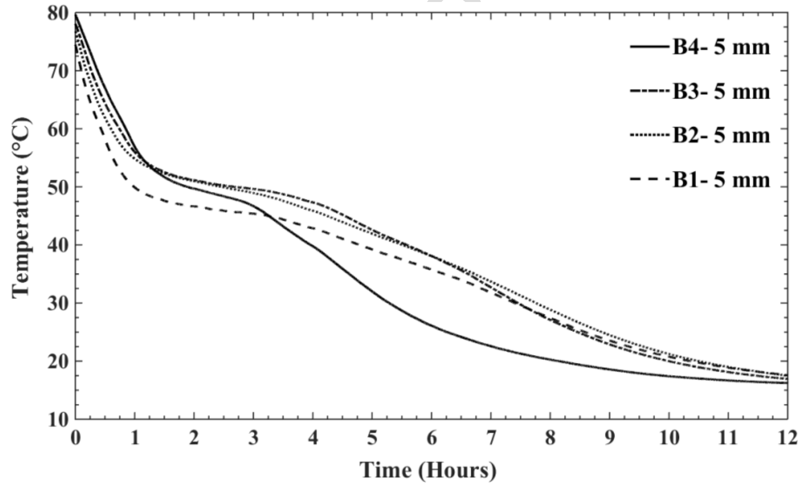

(b) Cylinder B

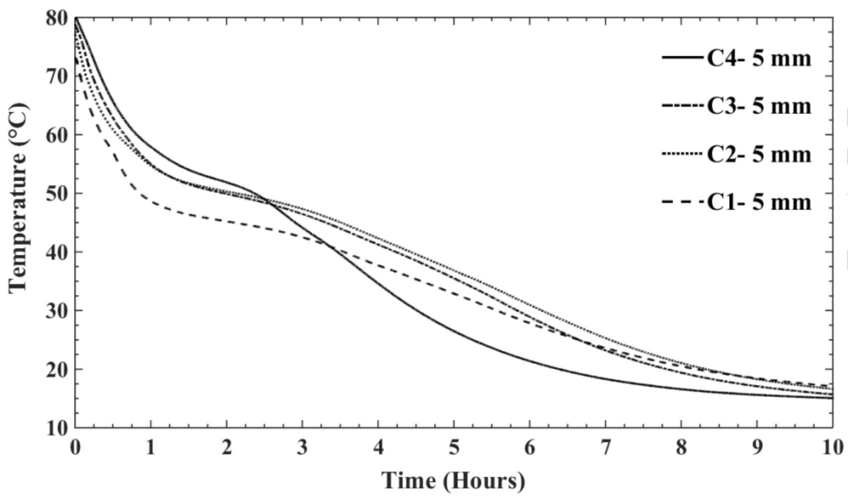

(c) Cylinder C

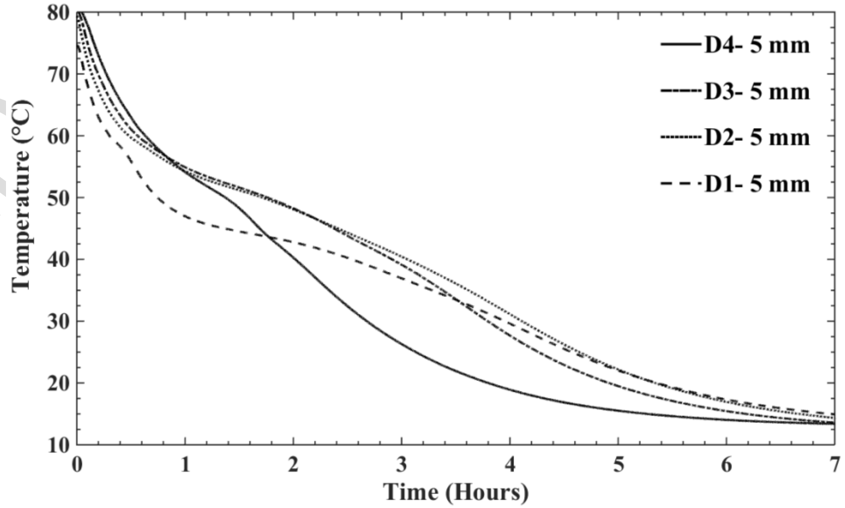

(d) Cylinder D

Fig. 8 Comparison of temperatures recorded by thermocouples located 5 mm away from the shells during the discharging process

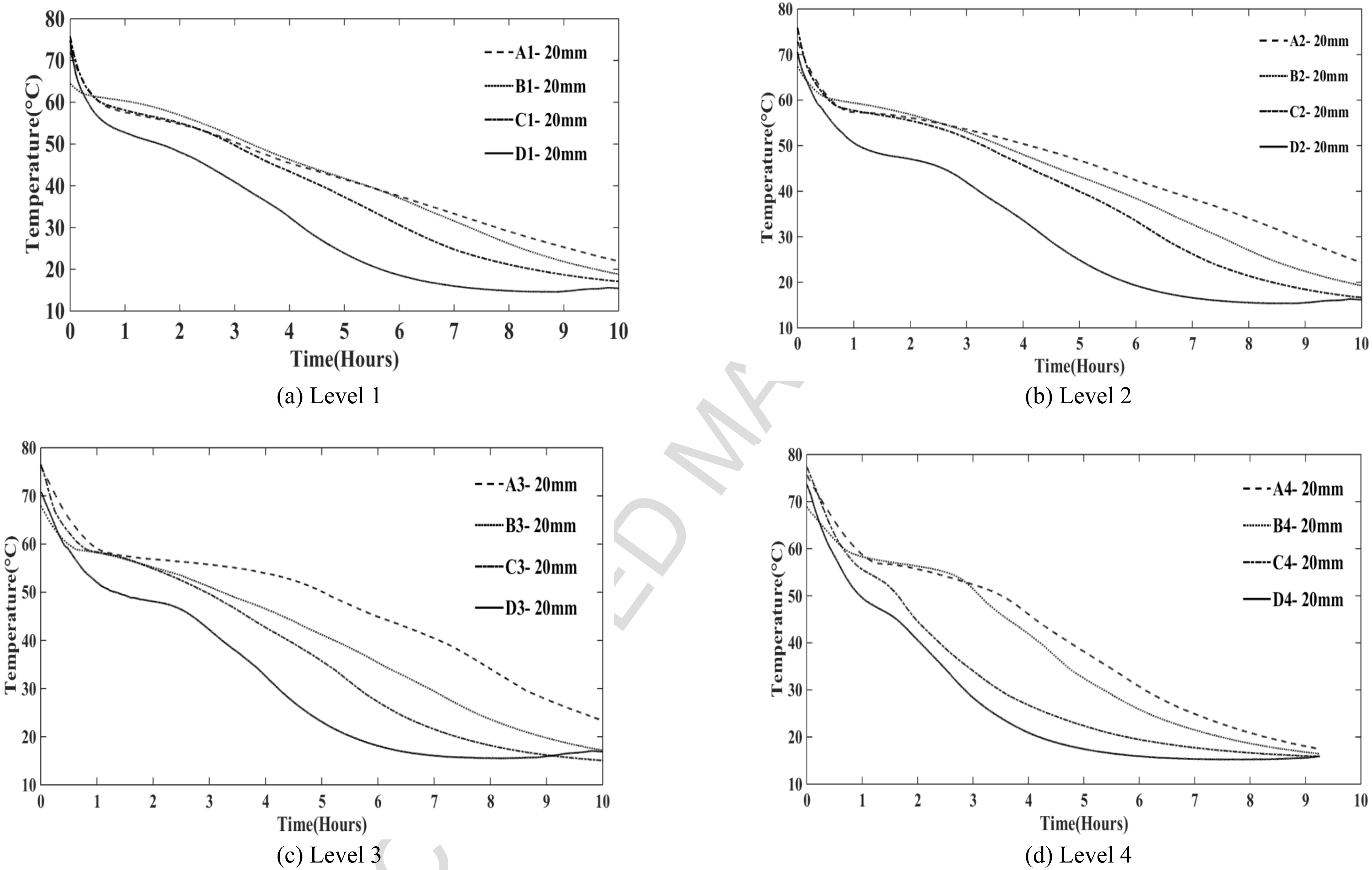

Fig. 9 Comparison of temperatures recorded by thermocouples located 20 mm away from the HTF tubes during the discharging process

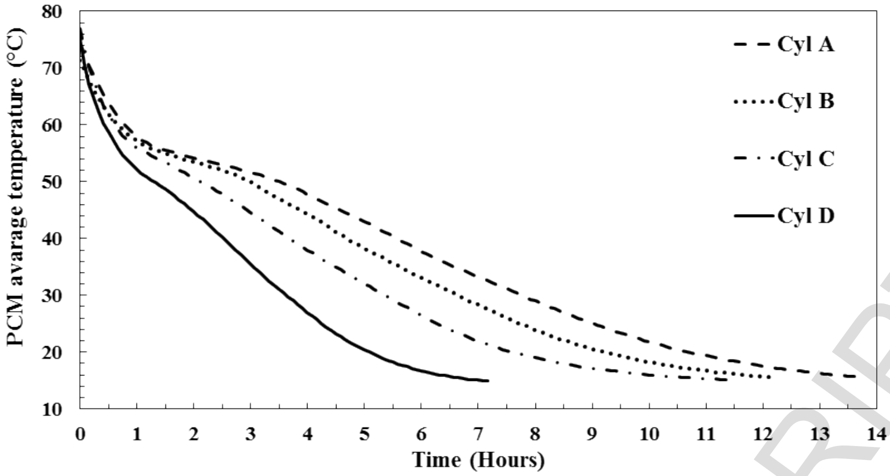

(a) Comparison of average PCM temperature

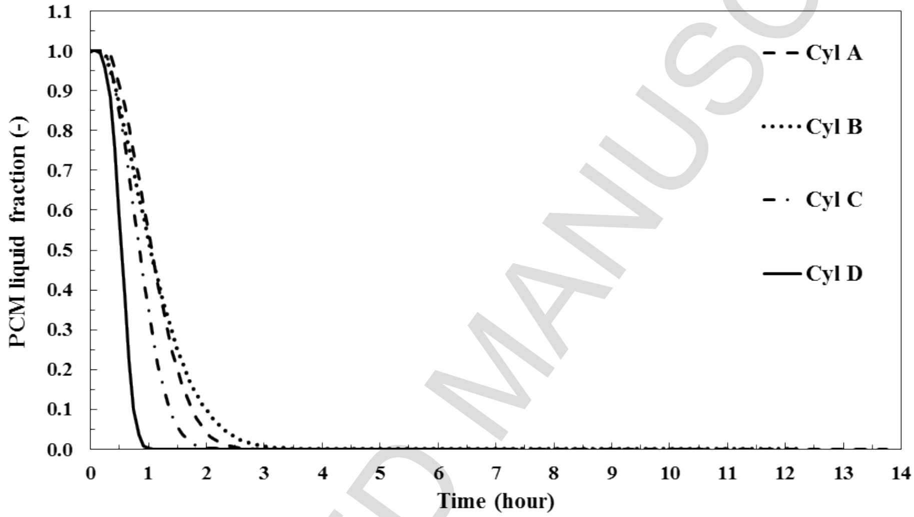

(b) Comparison of the PCM liquid fraction

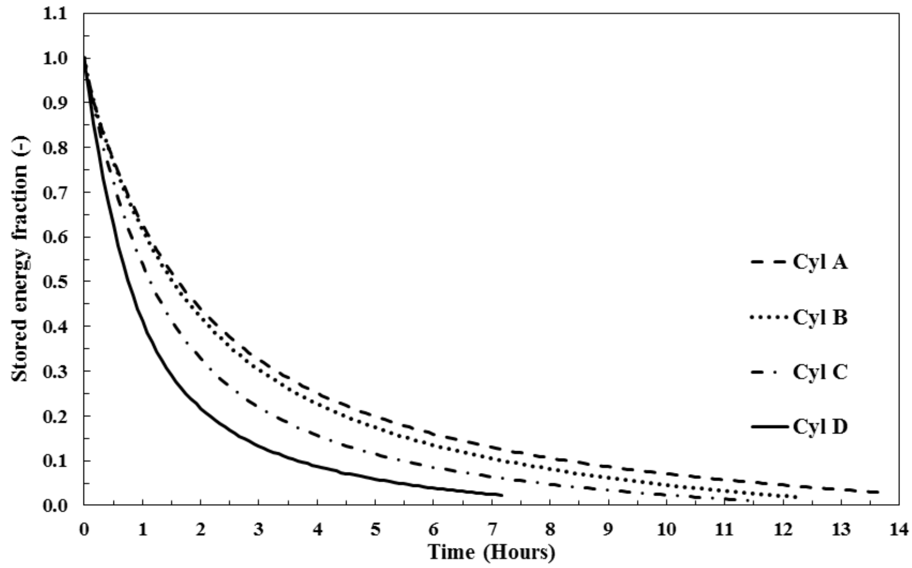

(c) Comparison of stored energy fraction

Fig. 10 Comparison of the PCM average temperature, liquid fraction, and stored energy fraction during the discharging process

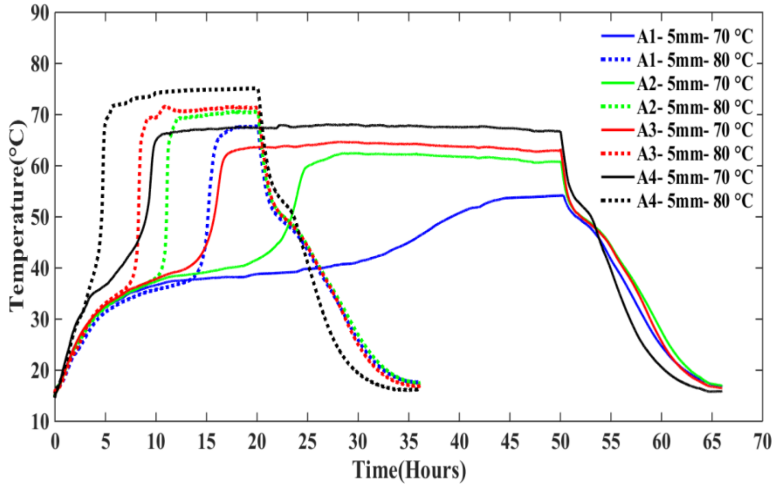

(a) Cylinder A

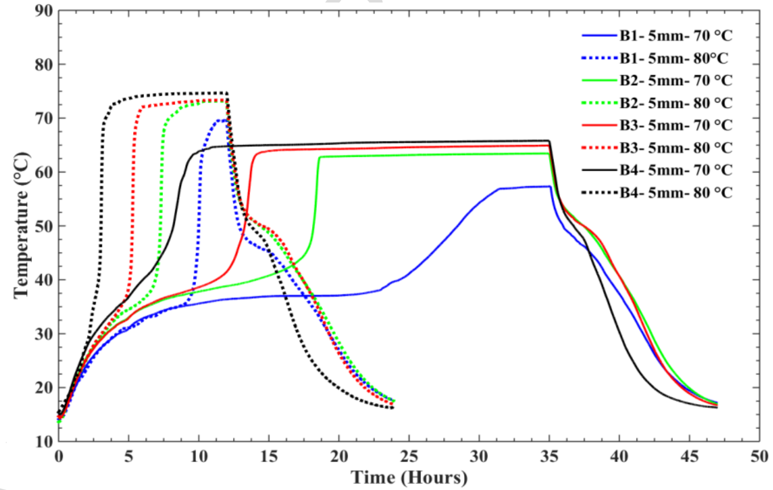

(b) Cylinder B

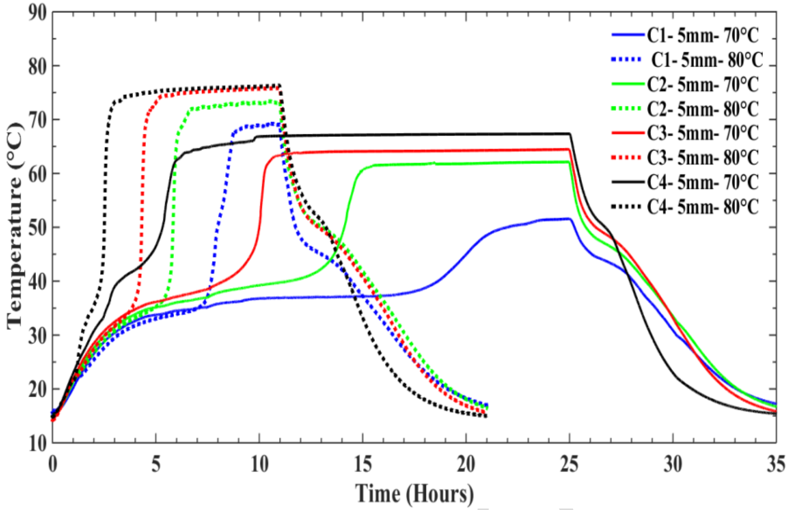

(c) Cylinder C

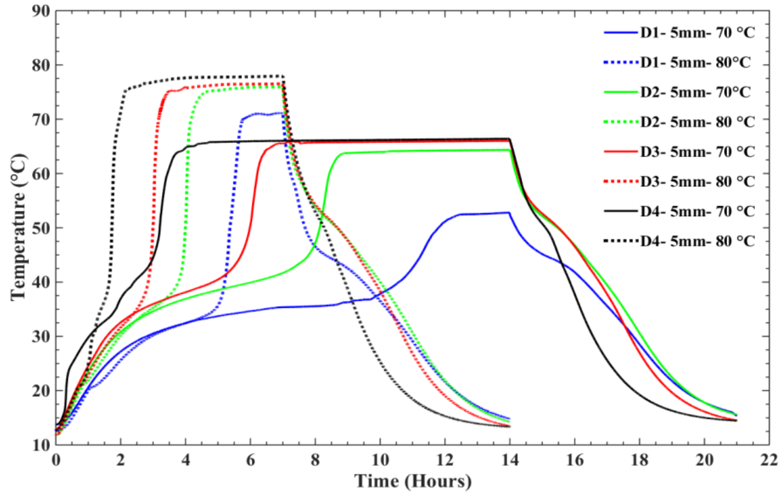

(d) Cylinder D

Fig. 11 Complete charging and discharging cycles for thermocouples located 5 mm away from the shells under different HTF temperatures

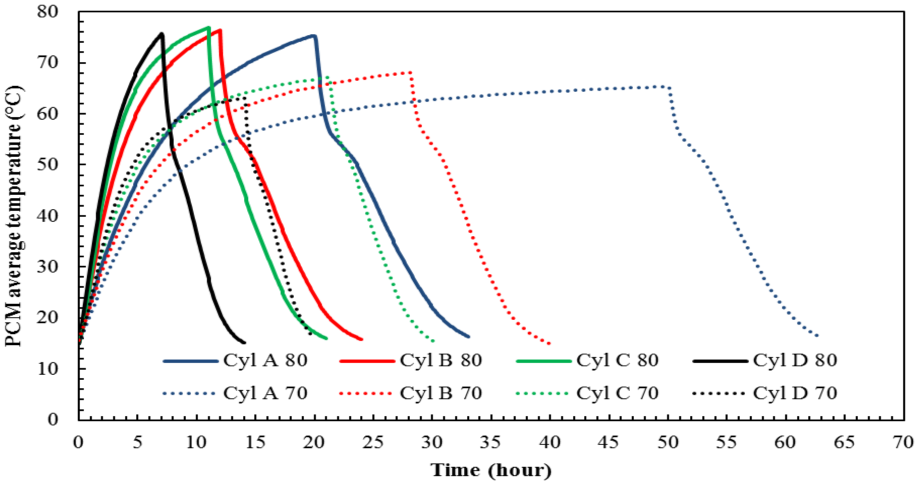

(a) Comparison of average PCM temperature

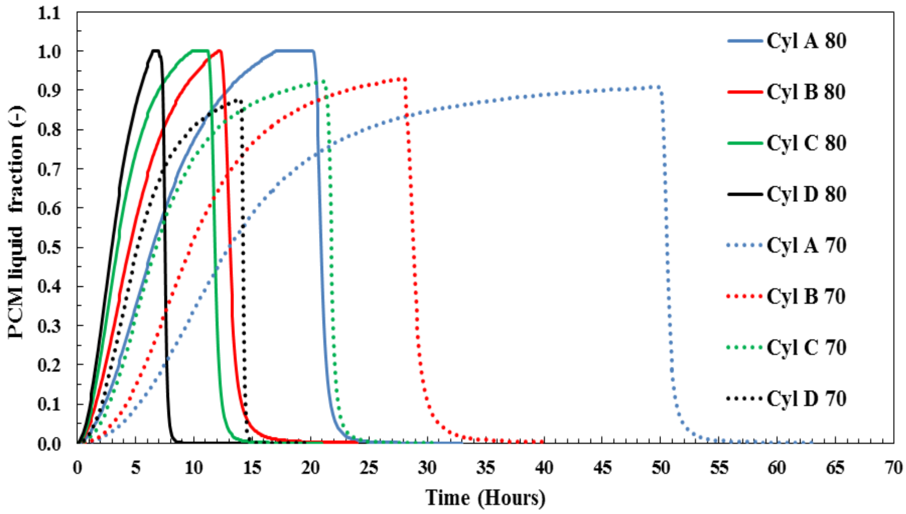

(b) Comparison of PCM liquid fraction

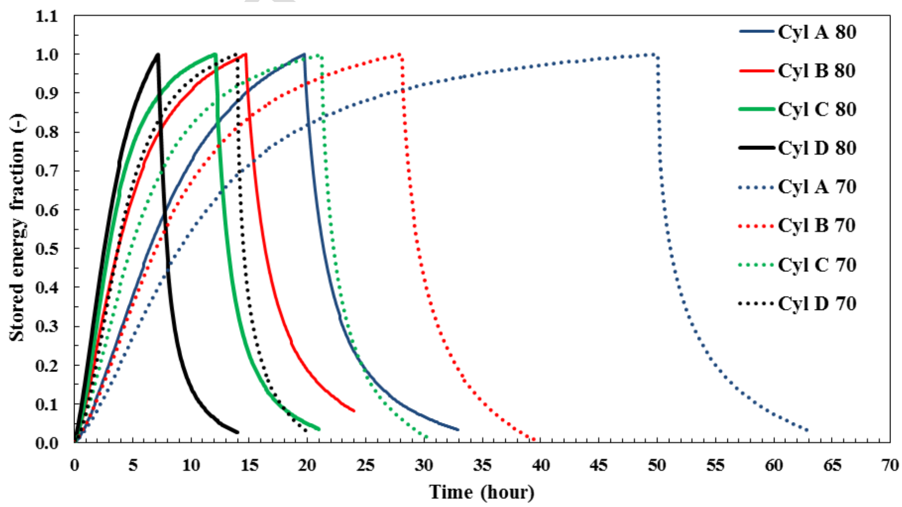

(c) Comparison of PCM liquid fraction

Fig. 12 Comparison of the PCM average temperature, liquid fraction, and stored energy fraction during the complete charging/discharging cycle

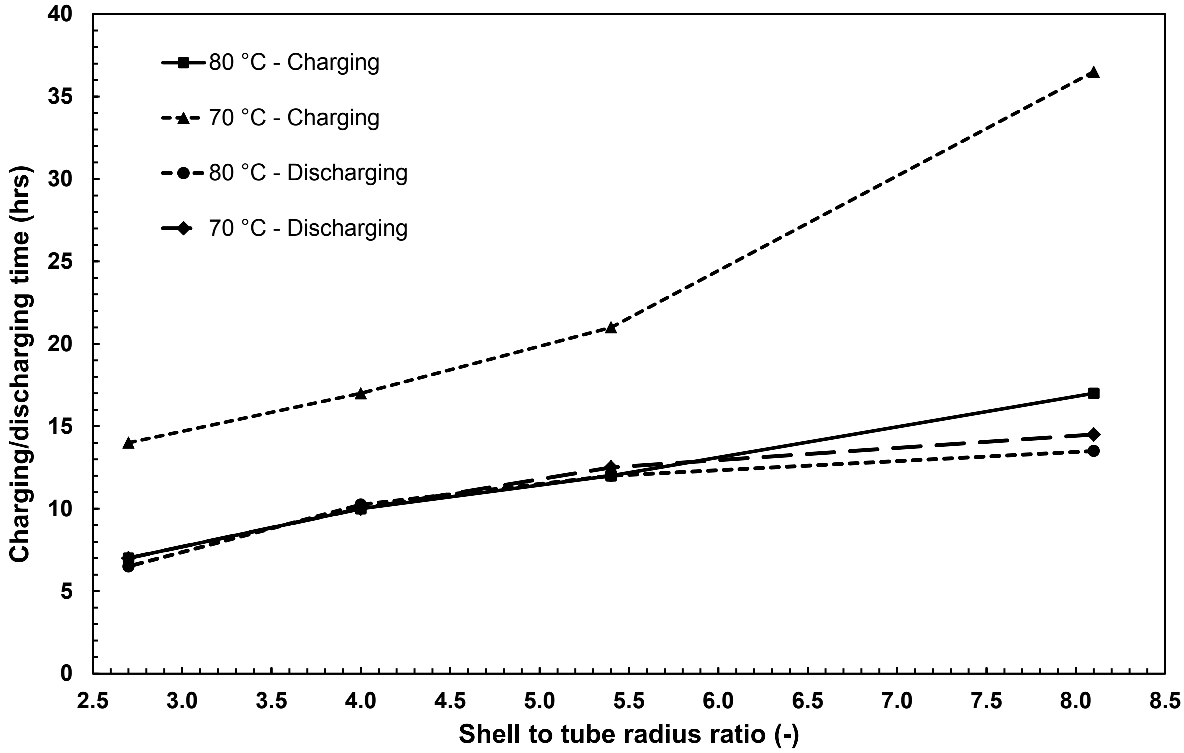

(a) Comparison of the charging and discharging time

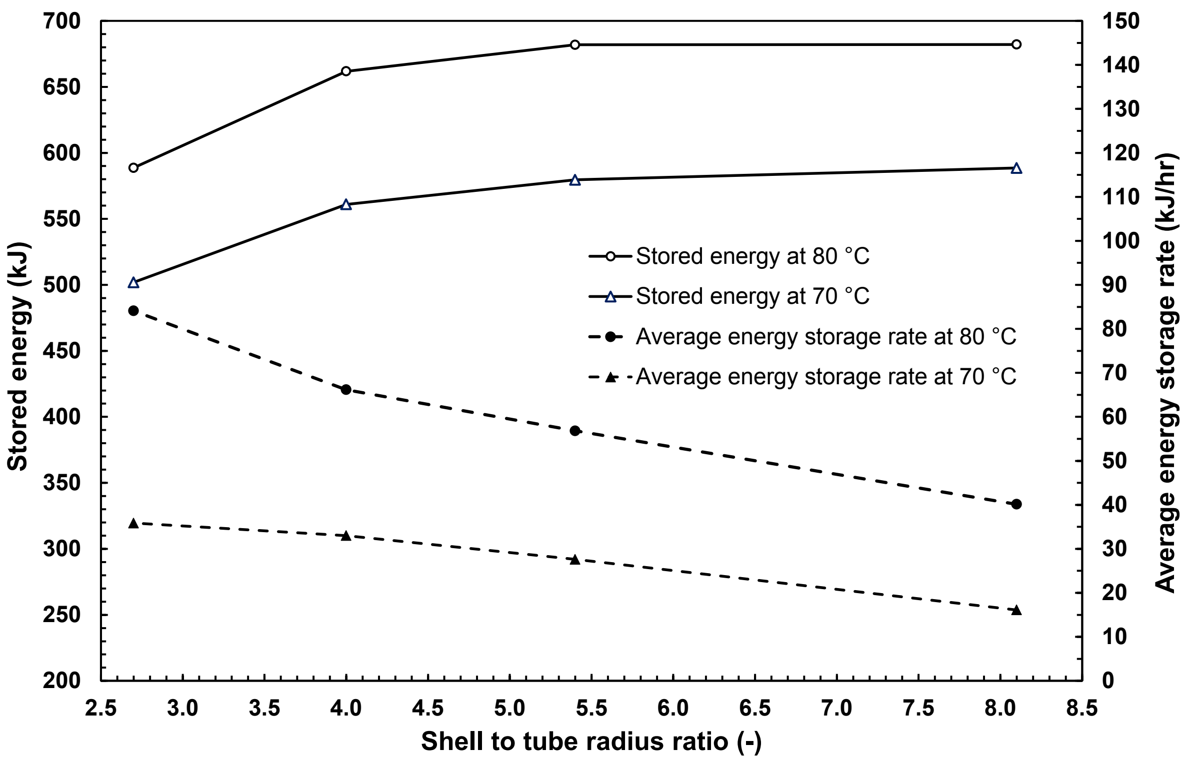

(b) Comparison based on stored energy and average energy storage rate

Fig. 13 The effect of the shell to tube radius ratio on the storage system performance under different HTF temperatures

Highlights

1. Thermal behaviour of vertical latent heat thermal energy storage systems was studied.
2. Effect of geometric and operating parameters was investigated using a weighting method.
3. The optimal shell to tube radius ratio of the LHTES system was evaluated.
4. The HTF flow rate had insignificant effect on the system storage performance.
5. The system storage performance increased substantially with the HTF temperature.

Table 1 Summary of the presented studies investigating shell-and-tube latent heat thermal energy storage systems

Reference	Study type		Geometric	Process		PCM	Phase change	Orientation	Geometric parameters				
	Numerical	Experimental	analysis	Charging	Discharging		temperature		R_i	R_o	R_o/R_i	L	L/R_i
[7]	✓		✓	✓		-	-	Horizontal	-	-	2 ~ 4.2	0.1	20 ~ 48
[8]	✓	✓	✓	✓		*n*-octadecane	27.55	Horizontal	0.00635	0.011 ~ 0.0183	-	1	-
[9]	✓	✓	✓	✓		*n*-octadecane	27.55	Horizontal	0.00635	0.011 ~ 0.0183	-	1	-
[10]	✓		✓	✓	✓	Lithium fluoride	849	Horizontal	0.01	0.024 ~ 0.052	-	2.4	-
[11]	✓		✓	✓	✓	Lithium fluoride	849	Horizontal	-	-	3 ~ 5	-	110 ~ 350
[12]	✓		✓	✓	✓	LiF-MgF_2	735	Horizontal	-	-	2.4 ~ 4.6	-	50 ~ 120
[13]	✓		✓	✓		$CaCl_2.6H_2O$	29.7 ~ 29.85	Vertical	0.016 ~ 0.04	0.033 ~ 0.082	-	3.2	-
						Paraffin	32 ~ 32.1						
						$Na_2SO_4.10H_2O$	39 ~ 39.15						
						Paraffin was	46.7 ~ 46.85						
[14]	✓		✓	✓		*n*-eicosan	36.4	Vertical	Constant	-	2 ~ 4.4	-	4 ~ 7
[15]	✓		✓	✓		*n*-eicosan	36.4	Vertical	-	-	1 ~ 6	-	-
[16]	✓	✓	✓	✓	✓	RT30	27.55	Vertical	0.0165	0.064	2.4 ~ 3.6	1	40 ~ 200
[17]	✓	✓		✓	✓	Technical grade paraffin	27.55	Vertical	0.0165	0.064	-	1	-
[18]		✓		✓		Paraffin wax	58 ~ 60	Vertical	0.0165	0.064	-	1	-

[19]		✓		✓	✓	Stearic acid	55.7 ~ 64.1	Vertical	0.0165	0.064	-	1	-
[20]	✓			✓	✓	LiF-CaF_2	767	Horizontal	0.0125	0.025	-	1.5	-
[21]	✓			✓	✓	*n*-octadecane	27.55	Horizontal	0.00635	0.01135	-	1	-
[22]	✓		✓	✓		LiF-CaF_2	767	Horizontal	0.0104 ~ 0.0178	0.024 ~ 0.028	-	1.5	-
[23]	✓			✓		LiF-CaF_2	767	Horizontal	0.0125	0.025	-	1.5	-
[24]		✓		✓	✓	Paraffin (P56-P58)	56 ~ 58	Horizontal	0.028	0.103	-	0.5	-
[25]	✓	✓		✓	✓	RT50	44.05 ~ 54.15	Horizontal	0.022	0.085	-	1	-
[29]	✓			✓	✓	*n*-octadecane	27.55	Horizontal	0.00635	0.0079	-	1	-
[30]	✓		✓	✓	✓	*n*-octadecane	27.55	Horizontal	0.00635	-	1.3 ~ 5	-	50 ~ 300
						Paraffin C_{18}	25						
						Polyglycol E600	22						
						$CaCl_2.6H_2O$	29.9						
						Gallium	29.76						
						Methyl palmitate	29						
[31]	✓		✓	✓	✓	Lead	54	Vertical	-	-	1.3 ~ 3	1 ~ 5	20 ~ 200
						H425	152						
						Li_2CO_3-K_2CO_3	232						

Table 2 Specifications of the investigated shell and tube systems

LHTES unit	Length	Shell radius	Tube radius	Radius ratio	Mass
	L **(m)**	R_o **(m)**	R_i **(m)**	R_o/R_i	***m*** **(kg)**
Cylinder **A**	0.5	0.0512	0.00635	8.1	3.12
Cylinder **B**	0.5	0.0512	0.00953	5.4	3.06
Cylinder **C**	0.5	0.0512	0.01270	4.0	2.97
Cylinder **D**	0.5	0.0512	0.01905	2.7	2.73

Table 3 Thermophysical properties and test conditions [35]

PCM		HTF		Dimension
Melting temperature	55-61	Charging temperature	70 and 80	°C
Congealing temperature	61-55	Discharging temperature	10	°C
Specific heat	2	Specific heat	4.18	kJ/kg.K
Thermal conductivity	0.2	Thermal conductivity	0.58	W/m.K
Solid density	880 (at 15 °C)	Density	998	kg/m^3
Liquid density	770 (at 80 °C)			kg/m^3
Latent heat of fusion	123.5			kJ/kg
Volume expansion	12.5			%
Dynamic viscosity	3.705×10^{-5}			kg/m.s

Table 4 Effect of the HTF flow rate on the charging, discharging, and the complete cycle time

		Same Re Number (23612), Different flow rates				Same flow rates (10 L/min), Different Re Number			
LHTES unit	Radius ratio	HTF flow rate (L/min)	Charging Time (hrs)	Discharging Time (hrs)	Complete cycle Time (hrs)	Re Number (-)	Charging Time (hrs)	Discharging Time (hrs)	Complete Cycle Time (hrs)
Cylinder A	8.1	5	50.11	15.05	65.16	47,225	50	15	65
Cylinder B	5.4	7.5	35.15	12.52	47.67	31,400	35	12.5	47.5
Cylinder C	4.0	10	25	10	35	23,612	25	10	35
Cylinder D	2.7	15	13.90	6.95	20.85	15,741	14	7	21